

Bar Formation During a Gaia-Sausage-Enceladus-like Merger Event

BIN-HUI CHEN ^{1,2,3,4,5} JUNTAI SHEN ^{2,3,4} AND PAOLA DI MATTEO ⁵

¹*Tsung-Dao Lee Institute, Shanghai Jiao Tong University, Shanghai 200240, People's Republic of China*

²*Department of Astronomy, School of Physics and Astronomy, Shanghai Jiao Tong University, 800 Dongchuan Road, Shanghai 200240, People's Republic of China*

³*State Key Laboratory of Dark Matter Physics, School of Physics and Astronomy, Shanghai Jiao Tong University, Shanghai 200240, People's Republic of China*

⁴*Key Laboratory for Particle Astrophysics and Cosmology (MOE) / Shanghai Key Laboratory for Particle Physics and Cosmology, Shanghai 200240, People's Republic of China*

⁵*LIRA, Observatoire de Paris, Université PSL, CNRS, 92195 Meudon, France*

ABSTRACT

Bars are among the most prominent galactic structures, yet their formation mechanisms remain incompletely understood. They can form either internally, via dynamical instabilities, or externally, triggered by interactions with other galaxies. The impact of mergers on bar formation and survival, however, has not been thoroughly investigated. To explore the influence of mergers on bars, we construct a suite of N -body merger pairs where a Gaia-Sausage-Enceladus-like radially biased satellite disk galaxy merges with a central disk galaxy during its bar formation. With the central galaxy fixed, the satellite varies in merger parameters: the mass ratio m/M relative to the central galaxy, the impact parameter b , and the orbital inclination angle θ_i relative to the central disk. We find that the bar survival probability decreases with increasing m/M . Mergers with $m/M \lesssim 1/10$ generally preserve the forming bar, whereas those with $m/M \geq 1/2$ tend to destroy it, producing more early-type-like remnants. For intermediate mass ratios ($1/5 \leq m/M \leq 1/3$), several models yield “weakening bars”, in which the bar survives the merger but gradually decays during subsequent secular evolution, possibly due to interactions between nested double bars formed from merger debris. In contrast to m/M , b and θ_i have only secondary and stochastic effects on bar survival. The different influences of these three merger parameters can be naturally explained by the tidal force exerted by the satellite on the forming bar, which tends to weaken the bar when the satellite crosses it nearly perpendicular to its major axis.

Keywords: Galactic bulge (2041), Galactic interactions (600), N-body simulations (1083)

1. INTRODUCTION

Bars are known to be prevalent in disk galaxies in the local universe (e.g., P. B. Eskridge et al. 2000; K. Menéndez-Delmestre et al. 2007; F. D. Barazza et al. 2008; K. Sheth et al. 2012; B. D. Simmons et al. 2014; P. Erwin 2018; Y. H. Lee et al. 2019), and the unprecedented capabilities of JWST have recently revealed many barred galaxies at high redshift as well (e.g., L. Costantin et al. 2023; Y. Guo et al. 2023; Z. A. Le Conte et al. 2024). Bars play a critical role in shaping their host galaxies, including driving corotation and Lindblad resonances (e.g., W. Dehnen 2000; M. Hayward et al. 2024), redistributing mass distribution (e.g., J. A. Sellwood 2014; V. P. Debattista et al. 2017; L.

Beraldo e Silva et al. 2023; B.-H. Chen et al. 2024), funneling gas toward galactic centers to feed central black holes (e.g., E. Athanassoula 1992; J. Kormendy & J. Kennicutt 2004; Z. Li et al. 2016, 2017; S. K. Kataria & M. Vivek 2024), exchanging angular momentum with the dark matter halo and heating stellar disks (e.g., E. Athanassoula 2002; J. A. Sellwood & J. J. Binney 2002; E. Athanassoula 2003a,b; I. Minchev & B. Famaey 2010; S. Long et al. 2014), contributing to the development of complex multi-populations of galaxies (e.g., V. P. Debattista et al. 2020; B.-H. Chen & Z.-Y. Li 2022), and so on. A comprehensive understanding of bar formation and evolution is therefore essential for advancing our knowledge of galactic physics.

The mechanism of bar structure formation remains an open question. Broadly, there are two formation pathways: internal formation, arising from dynamical instabilities of the galactic disk (e.g., A. Toomre 1981; J. A.

Sellwood 1981, 2016; M. S. Fujii et al. 2018; J. Binney 2020; J. Bland-Hawthorn et al. 2023; B.-H. Chen & J. Shen 2025; B.-H. Chen et al. 2025), and externally driven or promoted formation, triggered by interactions with neighboring galaxies (e.g., M. Noguchi 1987; M. Gerin et al. 1990; T. Miwa & M. Noguchi 1998; E. L. Lokas et al. 2014; Y. Zheng & J. Shen 2025; Y. Zheng et al. 2025). For the latter, the physical effects of a fly-by or merging satellite remain incompletely understood. Some studies suggest that tidal interactions may either facilitate or delay bar formation (E. L. Lokas et al. 2016; R. Moetazedian et al. 2017; T. Zana et al. 2018; A. R. Pettitt & J. W. Wadsley 2018; E. L. Lokas 2018); S. Ghosh et al. (2021) found that a minor merger can weaken an existing bar in some idealized N -body smooth particle hydrodynamics simulations, whereas A. Merrow et al. (2024) reported that a similar merger in one of the Auriga cosmological zoom-in simulations (R. J. J. Grand et al. 2017, 2024) can promote bar formation in a Milky Way-like galaxy.

As a typical disk galaxy, the Milky Way (MW) is known to host a bar structure (O. E. Gerhard & M. Vietri 1986; J. Binney et al. 1991; J. Shen et al. 2010; M. Ness & D. Lang 2016; M. Portail et al. 2017). With the advent of high-precision astrometric data from the *Gaia* mission (Gaia Collaboration et al. 2016, 2018, 2021, 2023), V. Belokurov et al. (2018) and A. Helmi et al. (2018) identified a population of inner halo stars with orbital and chemical properties distinct from the bulk of the Galactic disk (in hindsight, see also P. E. Nissen & W. J. Schuster 2010 for the identification of such stars before the *Gaia* era). The similarity in age and chemical abundance between such halo stars and those in external dwarf galaxies suggests an *ex situ* origin from a single ancient accreted satellite of these halo stars (e.g., M. Haywood et al. 2018; C. Gallart et al. 2019; C. Conroy et al. 2019a; P. Das et al. 2020; D. K. Feuillet et al. 2020; A. Bonaca et al. 2020). This accretion event, now widely recognized as the last major merger in the Galactic assembly history, is commonly referred to as the Gaia-Sausage-Enceladus (GSE) event. Since the seminal studies by V. Belokurov et al. (2018) and A. Helmi et al. (2018), the GSE has become a central topic in Galactic archaeology (e.g., G. C. Myeong et al. 2019; H. H. Koppelman et al. 2019; V. Belokurov et al. 2020; R. P. Naidu et al. 2020; M. Xiang & H.-W. Rix 2022; S. Khoperskov et al. 2023; M. Deng et al. 2024; H. Liu et al. 2025).

Therefore, as a barred galaxy that has experienced a significant merger, the Milky Way serves as a valuable test ground for investigating the relationship between galactic mergers and bar formation. Depending on the

timing relative to bar formation, merger events can be categorized as pre-bar-formation, during-bar-formation, or post-bar-formation. Despite debates (e.g., S. Nepal et al. 2024), many studies suggest that both the formation of the Galactic bar (J. Bovy et al. 2019; S. M. Wylie et al. 2022; J. L. Sanders et al. 2024; M. Haywood et al. 2024) and the GSE event (V. Belokurov et al. 2018; A. Helmi et al. 2018; M. Haywood et al. 2018; P. Di Matteo et al. 2019) occurred approximately $8 \sim 10$ Gyr ago, implying that the GSE might be a during-bar-formation merger event. However, whether the GSE event is responsible for the formation of the Galactic bar, or for promoting or suppressing it, remains poorly understood. As such, understanding galactic mergers, particularly those coinciding with the bar formation epoch, is critical for both constraining externally driven bar formation mechanisms and advancing Galactic archaeology. For instance, R. P. Naidu et al. (2021) constrained the properties of the GSE event by comparing simulations with observed kinematics and chemistry of GSE stars in the H3 Spectroscopic Survey (C. Conroy et al. 2019b).

In this study, we study the influence of during-bar-formation mergers on bar formation. We construct a suite of N -body merging pairs consisting of two similarly configured disk galaxies, possibly with different sizes, in which a satellite merges with a central galaxy while the latter is undergoing internal bar formation. With the same central galaxy, we vary the satellite with three merger parameters: (1) the satellite-to-central galaxy mass ratio m/M ; (2) the impact parameter b of the satellite’s incident velocity; and (3) the inclination angle θ_i between the merging orbital plane and the central galaxy’s disk plane. With these models, we systematically investigate how a GSE-like merger event—characterized by a radially biased orbit and spanning the plausible range of mass ratios inferred for the GSE event—affects bar formation in the central galaxy.

The structure of this paper is as follows. In Section 2, we describe the setup of the N -body merging pairs. Section 3 presents the main results regarding bar survival probabilities. In Section 4, we examine the dynamical mechanisms shaping the bar survival probabilities and discuss the bar weakening phenomenon. Finally, we summarize this paper in Section 5.

2. MODELS

We construct our models using the **AGAMA** package (E. Vasiliev 2019). Each system consists of a central and a satellite galaxy, both comprising a dark matter (DM) halo and a stellar disk. The DM halo follows a Navarro–Frenk–White (NFW) density profile (J. F.

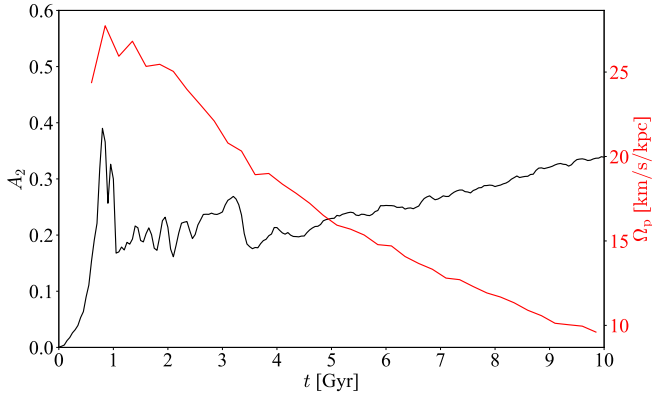


Figure 1. Temporal evolution of the bar strength A_2 (black) and pattern speed Ω_p (red) for the central galaxy evolved in isolation. A prominent bar forms within 1 Gyr and subsequently undergoes secular growth accompanied by a corresponding decline in pattern speed.

(Navarro et al. 1995, 1996) with an outer cutoff:

$$\rho_{\text{NFW}}(r) = \rho_0 \left(\frac{r}{a}\right)^{-1} \left(1 + \frac{r}{a}\right)^{-2} \times \exp\left[-\left(\frac{r}{r_c}\right)^2\right], \quad (1)$$

where r is the spherical radius, ρ_0 is the normalization constant set by the total halo mass, a is the halo scale length, and r_c is the outer truncation radius of the density profile.

The stellar disk is described by a quasi-isothermal distribution function (E. Vasiliev 2019):

$$f(\mathbf{J}) = \frac{\tilde{\Sigma}\Omega}{2\pi^2\kappa^2} \times \frac{\kappa}{\tilde{\sigma}_R^2} \exp\left(-\frac{\kappa J_R}{\tilde{\sigma}_R^2}\right) \times \frac{\nu}{\tilde{\sigma}_z^2} \exp\left(-\frac{\nu J_z}{\tilde{\sigma}_z^2}\right) \times \begin{cases} 1 & \text{if } J_\phi \geq 0, \\ \exp\left(\frac{2\Omega J_\phi}{\tilde{\sigma}_R^2}\right) & \text{if } J_\phi < 0, \end{cases} \quad (2)$$

where $\kappa/\nu/\Omega$ is the epicycle/vertical/circular frequency, J_R , J_ϕ , J_z are the actions, and

$$\begin{aligned} \tilde{\Sigma}(R) &= \Sigma_0 \exp(-R/R_d), \\ \tilde{\sigma}_R^2(R) &= \sigma_{R,0}^2 \exp(-2R/R_{\sigma_R}), \\ \tilde{\sigma}_z^2(R) &= 2h_z^2\nu^2(R), \end{aligned} \quad (3)$$

where R is the cylindrical radius, R_d is the disk scale length, h_z is the vertical scale height, Σ_0 is the central surface density, $\sigma_{R,0}$ is the central radial velocity dispersion, and R_{σ_R} is the scale length of the dispersion profile.

Part I of Table 1 lists the parameters of the central galaxy. This setup is typical for a cold disk model, which can form a bar spontaneously through bar instability (e.g., J. Shen et al. 2010; J. A. Sellwood & O. Gerhard

2020; T. Tepper-Garcia et al. 2021; J. Bland-Hawthorn et al. 2023; B.-H. Chen & J. Shen 2025; B.-H. Chen et al. 2025).

We employ the following parameters to quantify the bar structure:

$$\text{Bar strength } A_2 = \left| \frac{\sum_j m_j \exp(2i\phi_j)}{\sum_j m_j} \right|,$$

$$\text{Bar pattern speed } \Omega_p = \frac{\Delta\phi_2}{\Delta t},$$

where the bar phase angle is defined as

$$\phi_2 = \frac{1}{2} \arg\left(\frac{\sum_j m_j \exp(2i\phi_j)}{\sum_j m_j}\right).$$

Here, m_j and ϕ_j are the mass and cylindrical azimuthal angle of the j -th particle, respectively. Unless otherwise stated, the summations are taken over stellar particles with cylindrical radius $R < 15$ kpc.

Figure 1 shows the temporal evolution of the bar strength and pattern speed for the central galaxy evolved in isolation (hereafter, the “isolated model”). A prominent bar forms within 1 Gyr. With the secular growth of bar strength, the pattern speed declines at a rate approximately $2 \text{ km s}^{-1} \text{ kpc}^{-1} \text{ Gyr}^{-1}$, which is about half the estimated value of the Milky Way (R. Chiba et al. 2021).

For the merger models, the satellite’s parameters are scaled according to its mass ratio relative to the central galaxy:

Given $\gamma \equiv m/M$, then

$$\begin{aligned} m &= \gamma M, \\ N_p(\text{satellite}) &= \gamma N_p(\text{central}), \\ R_d(\text{satellite}) &= \gamma^{1/3} R_d(\text{central}), \\ h_z(\text{satellite}) &= \gamma^{1/3} h_z(\text{central}), \\ a(\text{satellite}) &= \gamma^{1/3} a(\text{central}), \\ R_{\sigma_R}(\text{satellite}) &= \gamma^{1/3} R_{\sigma_R}(\text{central}), \\ \sigma_{R,0}(\text{satellite}) &= \gamma^{1/3} \sigma_{R,0}(\text{central}). \end{aligned}$$

Here, the satellite’s velocity dispersion is inferred from the Tully–Fisher relation (R. B. Tully & J. R. Fisher 1977), which implies an approximate $\sigma \propto V_c \propto M^{1/3}$ scaling in the B band centered at $0.45 \mu\text{m}$ (J. Binney & S. Tremaine 2008). Although the Tully–Fisher relation exhibits intrinsic scatter in its power-law index (e.g., S. Courteau 1997; S. S. McGaugh et al. 2000), this uncertainty has a negligible effect on the subject under study (see Section 4.1).

The initial configurations of the merging pairs are illustrated in Figure 2. We vary only the key merger

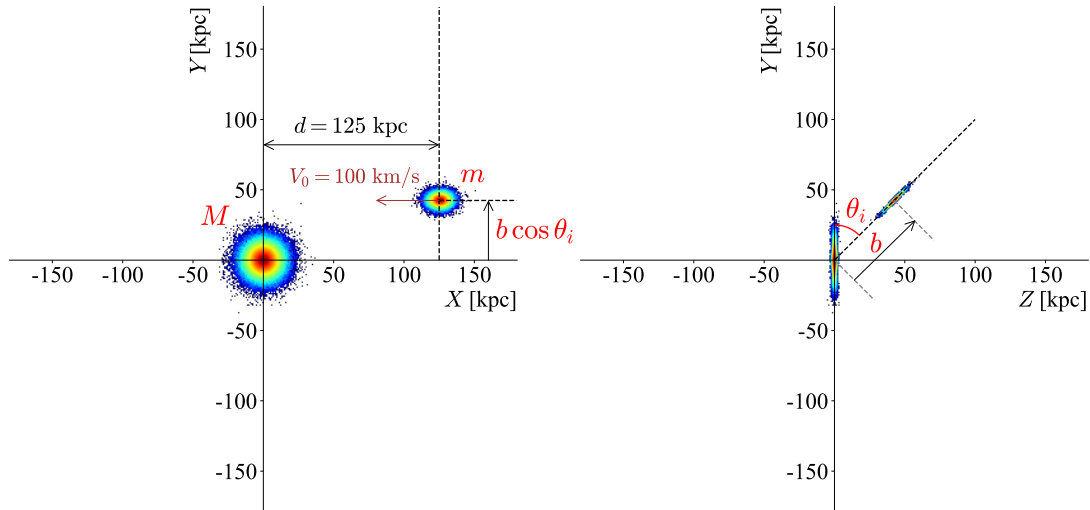


Figure 2. Illustration of the merger parameters with stereoscopic projections: the mass ratio m/M , impact parameter b , and orbital inclination angle θ_i . The initial separation between the two galaxies is fixed as $d = 125$ kpc along the X -axis, while the positions in other directions vary according to b and θ_i . The satellite’s incident velocity is fixed as -100 km/s along the X -axis.

Table 1. Simulation Configuration: Galaxy Components and Merger Parameters^a

Part I: Central Galaxy Parameters											
Component	M [$10^{10} M_{\odot}$]	N_p ^b	a or R_d [kpc]	r_c or h_z [kpc]	R_{σ_R} [kpc]	$\sigma_{R,0}$ [km/s]					
DM halo	100.0	1,000,000	20.0	200.0	–	–					
Stellar disk	5.0	1,000,000	2.5	0.25	5.0	100					
Part II: Merger Parameters											
Parameter	Values										
m/M	1/1	1/2	1/3	1/4	1/5	1/6	1/8	1/10	1/20		
b/kpc	-100	-80	-60	-40	-20	0	20	40	60	80	100
θ_i/deg	0	15	30	45	60	75	90				

^aPart I lists the structural properties of the central galaxy, while Part II gives the merger parameters.

^bParticle number.

parameters, as listed in Part II of Table 1: 9 values of the merger mass ratio m/M ; 11 values of the impact parameter b (negative for retrograde orbits); and 7 values of the inclination angle θ_i . This results in a total of 693 models. For each model, the satellite is initially placed at $\mathbf{P}_0 = (125 \text{ kpc}, b \cos \theta_i, b \sin \theta_i)$ with an incident velocity $\mathbf{V}_0 = (-100, 0, 0) \text{ km s}^{-1}$, which are chosen to ensure that the merger occurs on a radially biased orbit while the central galaxy is undergoing spontaneous bar formation. Note that, to reduce the dimensionality of the parameter space, we align the satellite’s disk plane with its orbital plane, which has no impact on our main conclusions (see Section 4).

We name these models as $\text{mr}\{M/m\}\text{ip}\{b\}\text{ia}\{\theta_i\}$ based on their merger parameters; for example, model

mr20ip-60ia45 is the case with $m/M = 1/20$, $b = -60$ kpc, and $\theta_i = 45^\circ$.

Each model is evolved using the **GADGET4** code (V. Springel et al. 2021) for 10 Gyr to ensure that the merger process and subsequent dynamical evolution thoroughly saturate. In most cases, the satellite merges with the central galaxy within about 1.5 Gyr after 2–3 pericentric passages. After the merger, the system evolves in a secular manner.

3. RESULTS

Figure 3 shows face-on views of the isolated model and several representative merger models at different epochs. In model mr20ip-60ia45 (second row), the satellite is very light and thus exerts a negligible influence on the

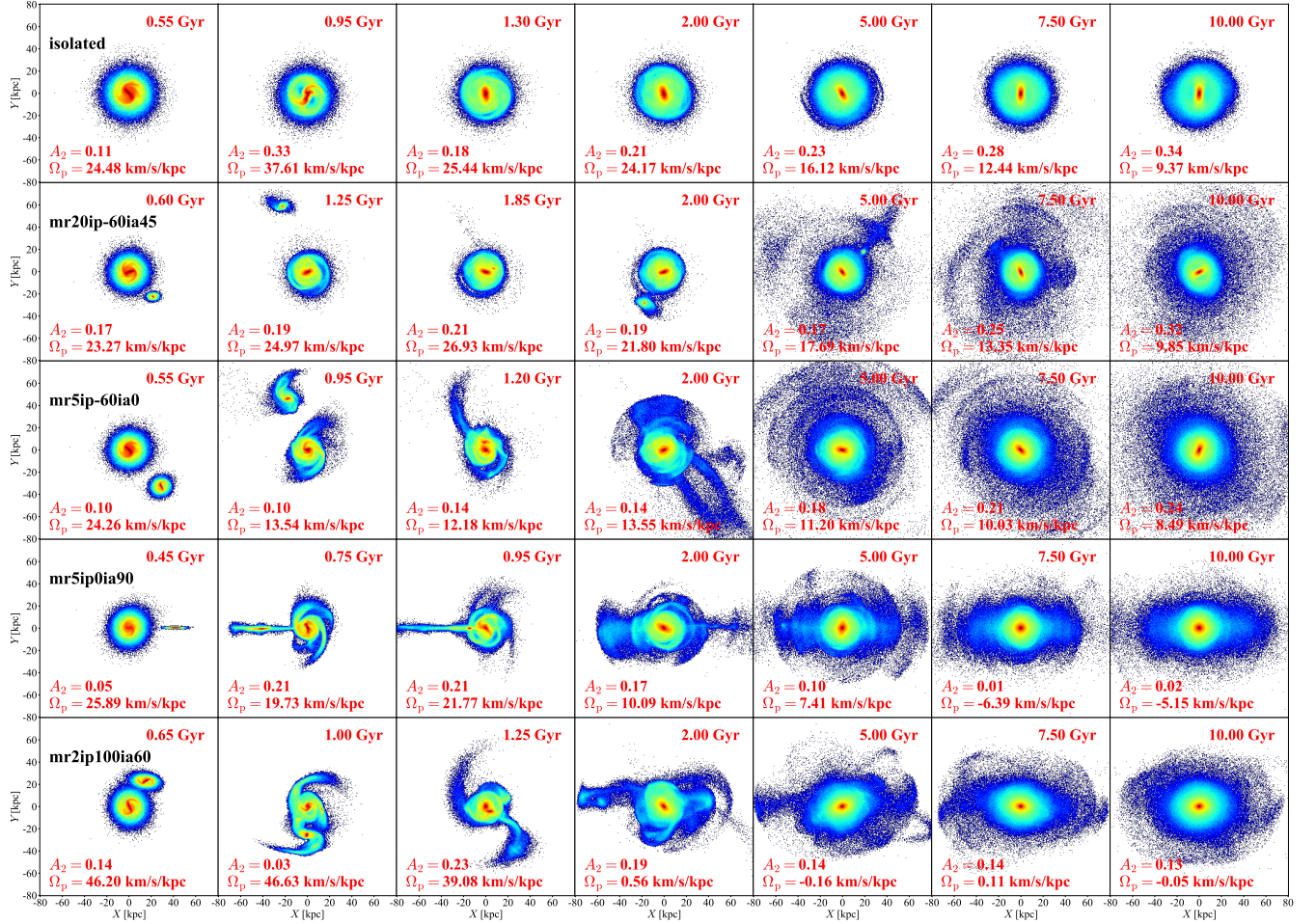


Figure 3. Face-on views of several representative models. The top row shows the isolated model. The second row depicts a minor merger, where the satellite’s effect on the bar is negligible. The third row presents a model in which the bar survives in a non-trivial merger. The fourth row illustrates a weakening bar that survives the merger but gradually decays subsequently in secular evolution. The fifth row shows a merger-produced elliptical-like system with negligible rotation, resulting from a violent merger. The bar strengths and pattern speeds of the central galaxy are annotated in the lower-left corner of each panel.

forming bar in the central galaxy. Consequently, the bar survives the merger, and its final morphology closely resembles that of the isolated model (top row). In model **mr5ip-60ia0** (third row), the bar is temporarily disturbed by the satellite but subsequently recovers. In contrast, in model **mr2ip100ia60** (fifth row), the satellite disrupts the forming bar, leaving behind an elliptical galaxy as expected for such a violent merger (O. E. Gerhard 1981; R. T. Farouki & S. L. Shapiro 1982; J. Negroponte & S. D. M. White 1983). An intermediate case appears in model **mr5ip0ia90** (fourth row), where the bar initially survives the merger but gradually decays over time, ultimately evolving into a featureless disk. Notably, many of these merger models exhibit shell-like structures formed by “phase wrapping” during the merger process (e.g., P. J. Quinn 1984).

To quantify the presence of a bar, we measure the bar strength of each model at every snapshot. Because the

satellite can tilt the disk of the central galaxy, we first realign the disk to its original plane before performing any bar-strength measurements. As illustrative examples, the bar strengths of the models in Figure 3 are annotated accordingly.

We find that some models evolve into elliptical systems without a genuine bar, yet still show a prominent A_2 signal—such as model **mr2ip100ia60** in Figure 3. A genuine bar exhibits significant pattern rotation, whereas in elliptical galaxies the apparent $m = 2$ mode has nearly zero rotation. To differentiate between these cases, we also measure the bar pattern speed for each model. In elliptical systems, the bar pattern speed—or more strictly, the $m = 2$ phase speed—is close to zero.

Figure 4 shows the distribution of bar pattern speed as a function of bar strength at the end of the simulation (10 Gyr). The models separate into two distinct

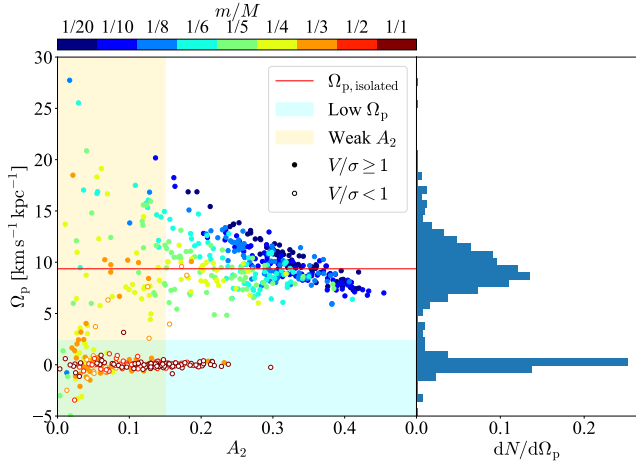


Figure 4. *Left:* Pattern speed Ω_p as a function of bar strength A_2 , with three models of very high pattern speed omitted for clarity (one with $\Omega_p \sim 40 \text{ km s}^{-1} \text{ kpc}^{-1}$ and two with $\Omega_p \sim 60 \text{ km s}^{-1} \text{ kpc}^{-1}$). The color of each point indicates the merger mass ratio. The red line marks the pattern speed of the isolated model, $\Omega_{p,\text{isolated}}$. The cyan and yellow shaded regions denote low pattern speeds ($\Omega_p < 0.25 \Omega_{p,\text{isolated}}$) and weak bars ($A_2 < 0.15$), respectively. Models with an average azimuthal streaming velocity-to-dispersion ratio $V/\sigma < 1$ within $10 < R/\text{kpc} < 20$ are shown as unfilled circles. *Right:* Histogram of Ω_p , showing one peak near $\Omega_{p,\text{isolated}}$ and another near $\Omega_p = 0 \text{ km s}^{-1} \text{ kpc}^{-1}$.

groups: one with pattern speeds near that of the isolated model, $\Omega_{p,\text{isolated}}$, and the other clustered around $\Omega_p = 0 \text{ km s}^{-1} \text{ kpc}^{-1}$. Models with $\Omega_p \simeq 0$ are typically early-type systems characterized by a relatively low azimuthal streaming velocity-to-dispersion ratio (averaged over $10 < R/\text{kpc} < 20$). Other models, particularly those with lower m/M , exhibit an anti-correlation between Ω_p and A_2 , reflecting the similar angular momentum in the bar region across models with similar merger orbits.

To exclude non-rotating early-type systems, we define a model as hosting a *genuine bar* at the end of the simulation if it satisfies: (1) $A_2 > 0.15$ and (2) $\Omega_p > 0.25 \Omega_{p,\text{isolated}}$, corresponding to the unshaded upper-right region of Figure 4.

Figure 5 presents the distribution of the final bar strength as a function of the merger mass ratio m/M , where models with $\Omega_p < 0.25 \Omega_{p,\text{isolated}}$ are marked as cross symbols. Overall, models with small satellites ($m/M \lesssim 1/10$) typically develop a prominent bar structure, with strengths comparable to or even exceeding that of the isolated model. As m/M increases, the final A_2 of the models generally decreases. When m/M reaches $1/4$, all models exhibit bar strengths lower than that of the isolated model. For even higher mass ratios,

nearly all models display either a weak A_2 or negligible rotation (marked as crosses), which indicates that in these cases, the massive satellites—regardless of their b or θ_i —violently disrupt the forming bar in the central galaxy.

To better visualize the trend that bars are more likely to be destroyed by more massive satellites, the left panel of Figure 6 shows the bar survival probability, \mathcal{P} , as a function of $M_{\text{satellite}}/M_{\text{central}}$, where in each mass ratio bin

$$\mathcal{P} \equiv \frac{N_{\text{bar}}}{N_{\text{total}}},$$

with N_{total} the number of models and N_{bar} the number of models hosting a bar at the end of the simulation. The blue points correspond to the initial mass ratio, $M_{\text{satellite}}/M_{\text{central}} = m/M$. Considering mass loss during the merger, the remaining satellite mass may be a more physically meaningful indicator than the initial mass. We estimate the “remaining mass” of the satellite using two definitions measured at the first apocenter of the merger: (1) the *bound mass* (orange points) is the total mass of stellar and dark matter particles gravitationally bound to the satellite, i.e., particles with

$$E_{\text{bound}} = \Phi_{\text{satellite}} + \frac{1}{2} v_{\text{in satellite}}^2 < 0,$$

and (2) the *core mass* (green points) is the stellar mass enclosed within 20 kpc of the satellite barycenter, where only stellar mass is used in calculating $M_{\text{satellite}}/M_{\text{central}}$. The left panel of Figure 6 demonstrates that the bar survival probability decreases systematically with increasing $M_{\text{satellite}}/M_{\text{central}}$ under all mass definitions. Nearly all bars survive mergers with $M_{\text{satellite}}/M_{\text{central}} \lesssim 0.1$, whereas almost all bars are destroyed when $M_{\text{satellite}}/M_{\text{central}} \gtrsim 0.4$, providing an upper limit on the possible merger mass ratio in the assembly history of a MW-like barred galaxy.

Notably, compared with the merger mass ratio, the bar survival probability shows little dependence on b or θ_i in Figure 5 (except for a weak secondary trend that, in models with $m/M \leq 1/8$, smaller $|b|$ is associated with slightly larger A_2). To better illustrate this, the right panel of Figure 6 presents the distribution of \mathcal{P} as a function of b and θ_i , where \mathcal{P} is calculated among models sharing the same b and θ_i . The nearly random distribution of \mathcal{P} in the panel demonstrates that these parameters are not primary in shaping the bar survival probability compared with the merger mass ratio. We also examine alternative proxies for the impact parameter, such as orbital circularity (by M. G. Abadi et al. 2003, 0–0.4 in our models) and ellipticity (0.7–1.0), and still find no significant dependence of bar survival on

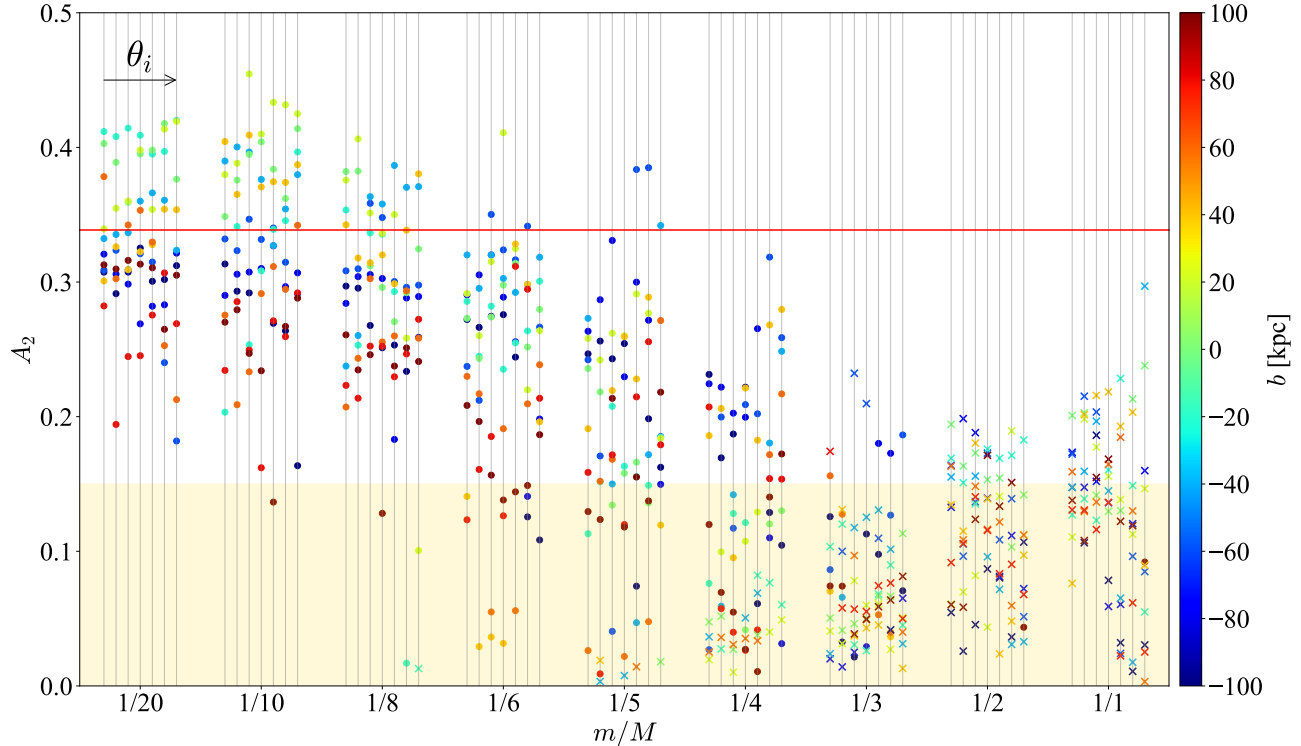


Figure 5. Distribution of final bar strength as a function of the merger parameters (m/M , b , θ_i). The mass ratio m/M is shown on the horizontal axis. At each value of m/M , the seven vertical lines correspond to different inclination angles θ_i , increasing from left to right (θ_i from 0° to 90°). The color of each point indicates the impact parameter b . The yellow shaded region marks the weak-bar regime, defined as $A_2 < 0.15$. For comparison, the final bar strength of the isolated model is indicated by the red horizontal line. Models with negligible pattern speed ($\Omega_p < 0.25 \Omega_{p,\text{isolated}}$) are shown as crosses and are primarily located at higher m/M .

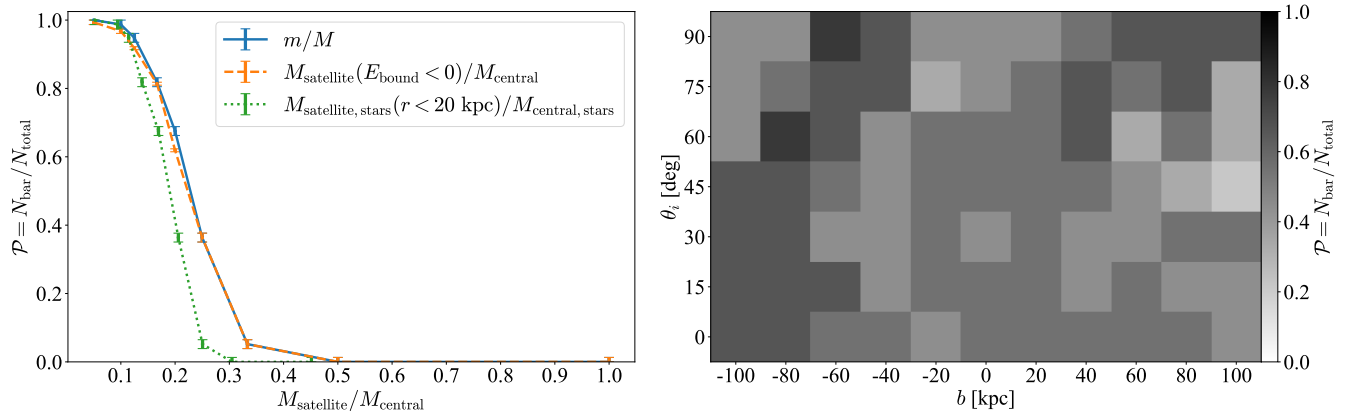


Figure 6. **Left:** Bar survival probability as a function of the satellite-to-central galaxy mass ratio, shown for three definitions: the initial mass ratio m/M (blue), the bound mass of the satellite relative to the total mass of the central galaxy (orange), and the satellite's core stellar mass (within 20 kpc around its baryonic center) relative to the central galaxy's total stellar mass (green). In each mass ratio bin, N_{total} is the total number of models, and N_{bar} is the number of models hosting a bar at the end of the simulation. Vertical error bars indicate Poisson uncertainties in each bin. **Right:** Similar to the left panel, but showing the bar survival probability (indicated by the color of each pixel) as a function of b and θ_i . In each pixel, \mathcal{P} is calculated among all m/M models sharing the same b and θ_i .

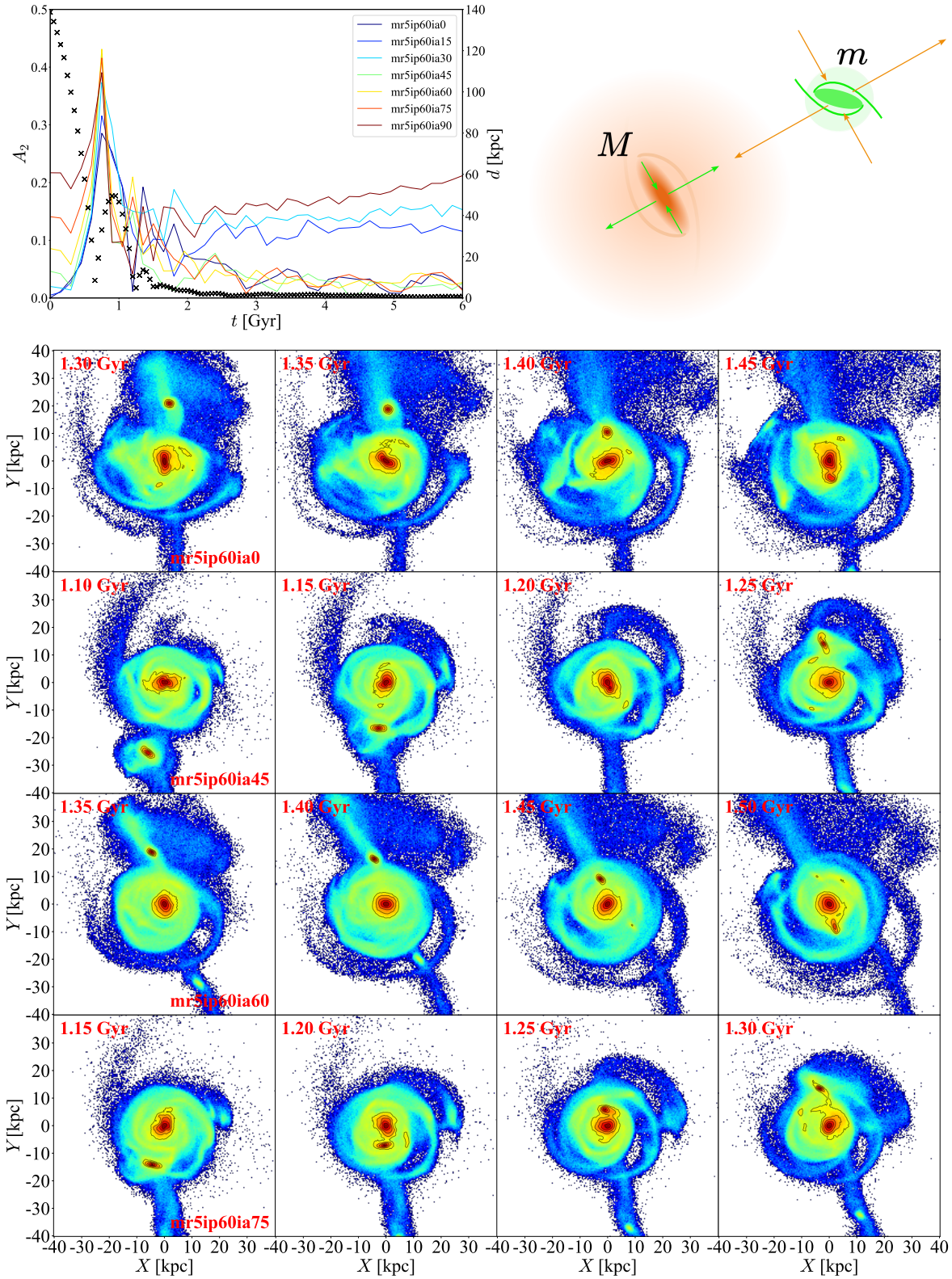


Figure 7. **Upper left:** Evolutionary histories of the bar strength $A_2(t)$ shown as solid lines and the distance $d(t)$ between the galactic centers shown as crosses (averaged across these models). All models share the same merger mass ratio and impact parameter, but evolve toward distinct barred or unbarred morphologies by 6 Gyr. **Lower rows:** Face-on views of the non-barred models in the *mr5ip60iaX* series. All exhibit severely deformed bars due to strong tidal disturbances from the satellites. **Upper right:** Schematic illustration of the tidal interaction between the central galaxy (orange) and the satellite (green).

either proxy. Therefore, in our simulations, the bar survival probability is determined primarily by the merger mass ratio and shows no notable dependence on b , θ_i , or related orbital parameters.

4. DISCUSSION

4.1. Influence of b and θ_i on the forming bar

Section 3 shows that bar survival probability during mergers is governed primarily by the merger mass ratio. In the intermediate regime, $0.10 \lesssim m/M \lesssim 0.40$, the survival probability lies between 0 and 1, indicating that bars survive in some mergers with particular combinations of b and θ_i but are destroyed in others. This indicates that b and θ_i play a secondary, albeit stochastic, role in determining whether a bar survives a given merger.

For example, the upper left panel of Figure 7 shows the bar evolutionary histories of models `mr5ip60iaX` along with $d(t)$ the distance between the galactic centers. These models share the same merger mass ratio and impact parameter, and thus follow similar merging orbits. Therefore, we plot only the averaged $d(t)$ across these models. They all exhibit two passages between 0 Gyr and 2 Gyr before transitioning into secular evolution as the intergalactic distance approaches zero. Despite their similar orbits, the models show remarkably different bar evolution: some develop prominent bars by the end, while others do not. Given the similar merger orbits, this divergence in bar evolution must arise from some subtle differences in the merger process that ultimately shape the final barred or unbarred morphologies.

To identify the subtle factors responsible for the divergent bar evolution, the lower rows of Figure 7 present several key snapshots of the non-barred models identified in the upper left panel, tracing the bar destruction process in each case. The snapshots show that the satellites cross the forming bars along directions nearly perpendicular to the bar’s major axis at certain times (possibly between the displayed snapshots). During these passages, the satellites induce strong disturbances, evident in the significantly distorted bars, which ultimately deconstruct the forming bars in these models.

The tidal forces exerted by the satellite on the primary galaxy and the forming bar can account for such violent disturbances. The upper right panel of Figure 7 illustrates the physical impact of the tidal force during a merger. The satellite exerts an extensive tidal force along the axis connecting the galactic centers, while a compressive force acts in directions perpendicular to it. If the bar’s major axis is aligned perpendicular to this axis, it experiences compression along its major axis and extension along the orthogonal directions, tending to cir-

cularize the structure. This expectation is consistent with the morphological distortions shown in the lower rows. When the infalling satellite passes near the bar’s minor axis, it can distort the forming bar into a rounder shape. Thus, a satellite on an orbit nearly perpendicular to the bar can exert a tidal force capable of deconstructing it. Whether the bar is ultimately destroyed depends on the tidal force strength, $F_{\text{tidal}} \propto m/d^3$, time span of the nearly perpendicular passage, and the robustness of the bar structure against external perturbations. Figure 7 shows cases in which the satellite’s tidal influence is strong enough to destroy the forming bar.

This physical picture explains the dependency of bar survival probability on the three merger parameters. The influence of b and θ_i is stochastic: the tidal force disrupts the bar only when the satellite happens to align nearly perpendicular to the bar’s major axis for a sufficient duration while crossing the bar. Even in such cases, only sufficiently massive satellites can exert a strong enough tidal perturbation to disrupt the bar as the tidal force scales as $F_{\text{tidal}} \propto m$. For a tiny satellite, with $m/M \lesssim 1/10$, almost every bar can survive the merger. As the satellite mass increases, both the strength and the spatial and temporal extent of the bar-destructive tidal force grow, making bar destruction more likely during the merger. With even higher satellite mass, for $m/M \geq 1/2$, even the disk can be strongly distorted or destroyed, explaining why nearly all bars are disrupted in such models.

Notably, the above physical framework is purely dynamical and does not depend on whether the merger occurs during or after bar formation, nor on the presence of a gas component. The only requirement is that the central galaxy hosts a (formed or forming) bar pattern capable of interacting with the merging satellite. Consequently, this explanation should also apply to post-bar-formation merger events (with or without gas), where we expect a similar dependence of the bar survival probability on $(m/M, b, \theta_i)$. For example, with post-bar-formation mergers that include a non-trivial gas component, Y. F. Zhou et al. (2025) demonstrate qualitatively similar results.

4.2. Weakening bars

Figure 3 shows that the merger event in model `mr5ip0ia90` does not completely destroy the bar. However, the bar gradually weakens after the merger and eventually disappears. A similar phenomenon, referred to as a bar-weakening event, has been reported in minor mergers by S. Ghosh et al. (2021). Here, we define a (significantly) weakening bar based on the following criteria:

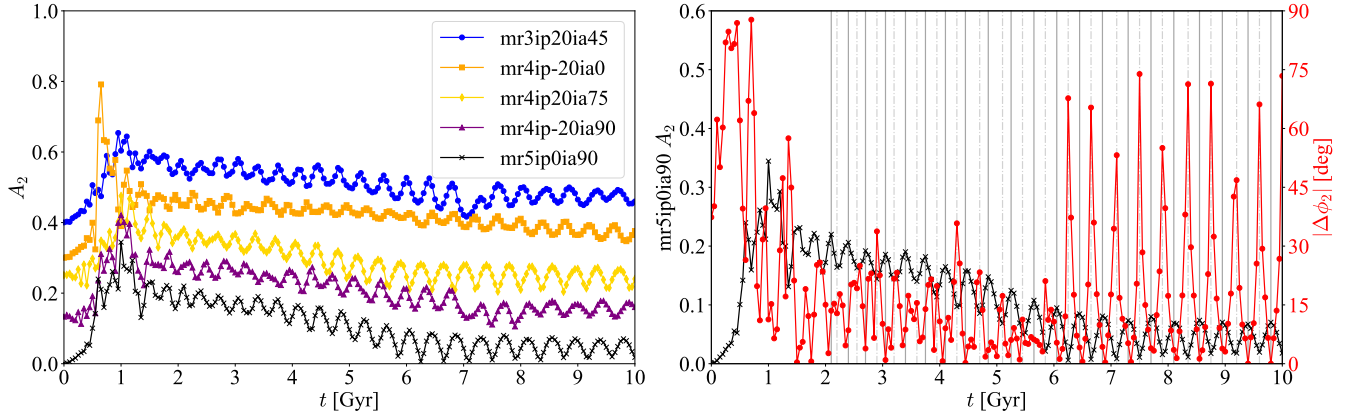


Figure 8. **Left:** $A_2(t)$ curves of the weakening bars. For clarity, the curves are vertically offset by 0.1 from each other. **Right:** Evolution of A_2 in model mr5ip0ia90, alongside $m = 2$ phase deviations between the inner ($R < 7.5$ kpc) and outer ($7.5 \text{ kpc} < R < 15$ kpc) bar regions. After the merger ($t \gtrsim 2$ Gyr), the maxima and minima of A_2 are marked by vertical gray solid and dashed lines, respectively. The minima of A_2 align with maxima of $|\Delta\phi_2|$ approximately, indicating a tight correlation between bar strength and double-bar interaction.

- Right after the merger, the system hosts a prominent bar: $A_{2,m} > 0.15$, where $A_{2,m} \equiv \text{mean}\{A_2(t) : 2 \text{ Gyr} < t < 3 \text{ Gyr}\}$.
- The final bar strength is significantly decreased relative to the value right after the merger: $A_{2,f} < 0.5 A_{2,m}$.
- The final snapshot lacks a prominent bar: $A_{2,f} < 0.15$.

Among the 693 merger models, we identify 5 cases exhibiting significant bar weakening, with their $A_2(t)$ curves shown in the left panel of Figure 8. An additional 8 models show milder weakening if we relax condition (b) from $0.5 A_{2,m}$ to $0.75 A_{2,m}$ and remove condition (c). They account for approximately 0.7% and 1% of all models, respectively, indicating that bar weakening is a rare phenomenon. All identified bar weakening models fall within the range $1/5 \leq m/M \leq 1/3$, corresponding to the intermediate regime in the probability curves of Figure 6.

A possible cause of the weakening bars is the interaction between the nested double bars in these models. As shown in the left panel of Figure 8, in addition to the secular decline in bar strength after the merger, the bar strength exhibits periodic oscillations. Inspection of the face-on views reveals that these models develop double-bar features, formed from clumpy merger debris (rather than internal dynamical instabilities as in V. P. Debattista & J. Shen 2007, J. Shen & V. P. Debattista 2009, and M. Du et al. 2015). For example, model mr5ip0ia90, quantified by the right panel of Figure 8, presents the phase deviation $|\Delta\phi_2|$ between the inner ($R < 7.5$ kpc) and outer ($7.5 \text{ kpc} < R < 15$ kpc) bar regions showing a significant offset, which indicates the presence of a double-bar pattern. Notably, although

with some noise, the bar strength $A_2(t)$ usually reaches minima when the phase deviation reaches maxima. Similar behaviors are seen in other bar weakening models, suggesting a strong correlation between bar strength evolution and the relative phase of the nested bars. This phenomenon resembles the double-bar interaction described by V. P. Debattista & J. Shen (2007) and J. Shen & V. P. Debattista (2009), who directly constructed isolated double-barred galaxy models. In their run 1, a similar bar weakening process was observed: the dominant bar pattern gradually decreased from above 0.25 to below 0.1, also accompanied by periodic oscillations. Oscillations in bar strength were also notable in the double-bar models of M. Du et al. (2015) and the weakening bar models of S. Ghosh et al. (2021). These similarities suggest that the weakening is likely driven by dynamical interaction between the inner and outer bars. Thus, phenomenologically, the coupled evolution of nested bars appears to be responsible for both the oscillations and the secular decline in bar strength in these models.

Other processes, such as central mass concentration and angular momentum exchange discussed by S. Ghosh et al. (2021), may also contribute to bar weakening. However, given the similarity in frequency between the rapid oscillations of the $A_2(t)$ curves and the double-bar phase deviations, the weakening bars in our models appear more consistent with mutual interactions between nested double bars.

The interaction between nested bars provides a natural explanation for the low probability of forming bar weakening models. Such interactions arise only when a merger event coincidentally produces a double-bar system, allowing the inner and outer bars to interact and

undermine the global bar strength. This scenario also explains why bar weakening models occur within the merger mass-ratio range $1/5 \leq m/M \leq 1/3$: if the satellite is too massive, the forming bar is directly disrupted by the merger; if it is too small, it cannot produce a prominent double-bar pattern. Consequently, bar weakening is confined to the transitional regime of the bar survival probability curves shown in Figure 6.

Note that while interactions between nested bars provide a plausible mechanism for bar weakening, they do not always lead to a decline in bar strength. For example, in run 2 of V. P. Debattista & J. Shen (2007) and the clumpy double-bar model of M. Du et al. (2015), the nested bars induce periodic oscillations in bar strength without significantly weakening the global bar strength. The conditions under which such interactions can weaken a bar remain to be explored. A detailed investigation of this topic is beyond the scope of the present work and will be addressed in a follow-up paper.

In summary, the bar weakening events identified in our models are likely driven by interactions between nested bars, which occur occasionally in the transitional regime of the bar survival probability curve.

5. SUMMARY

We have constructed 693 N -body models of GSE-like radially baised major merger events, each consisting of a central and a satellite disk galaxy, with varying merger mass ratios m/M , orbital impact parameters b , and orbital inclination angles θ_i . The satellite’s initial conditions are set up so that it merges into the central galaxy around 1.5 Gyr, during the spontaneous bar formation process of the central galaxy.

We find that the bar survival probability decreases primarily with increasing m/M (Figure 6). Bars nearly always survive mergers with $m/M \lesssim 0.1$, but are never preserved in mergers with $m/M \geq 0.5$, where the galaxies evolve into more early-type-like systems that may appear as non-rotating bar-like ellipticals (Figures 3 and 4). Within the transitional regime between definite bar

survival and destruction ($1/5 \leq m/M \leq 1/3$), several models show bar weakening phenomenon (Figure 8), possibly driven by interactions between nested double bars formed from merger debris (Section 4.2).

In contrast, the impact parameter b and inclination angle θ_i exert secondary and stochastic effects on bar survival compared with m/M . The tidal force exerted by the satellite on the forming bar naturally explains the dependencies of bar survival probability on these three merger parameters (Section 4.1). This tidal interaction is purely dynamical and therefore independent of whether it occurs during-bar-formation or post-bar-formation, or of the presence of gas content, implying that post-bar-formation and gas-rich mergers may also follow similar behavior.

ACKNOWLEDGMENTS

We thank the anonymous referee for the careful review. We sincerely thank Victor P. Debattista, Zhao-Yu Li, and Hui Li for helpful discussions. Bin-Hui Chen gratefully acknowledges the financial support from the China Scholarship Council, the support of the T.D. Lee Scholarship, and the sponsorship from Yangyang Development Fund. The research presented here is partially supported by the National Natural Science Foundation of China under grant Nos. 12533004, 12025302, 11773052; by China Manned Space Program with grant no. CMS-CSST-2025-A11; by the “111” Project of the Ministry of Education of China under grant No. B20019; and by Office of Science and Technology, Shanghai Municipal Government with grant Nos. 24DX1400100 and ZJ2023-ZD-001. This work used the Gravity Supercomputer at the Department of Astronomy, Shanghai Jiao Tong University, and the facilities in the National Supercomputing Center in Jinan.

Software: AGAMA (E. Vasiliev 2019), GADGET-4 (V. Springel 2005; V. Springel et al. 2021), Numpy (C. R. Harris et al. 2020), Scipy (P. Virtanen et al. 2020), Matplotlib (J. D. Hunter 2007), and Inkscape.

REFERENCES

- Abadi, M. G., Navarro, J. F., Steinmetz, M., & Eke, V. R. 2003, *ApJ*, 597, 21, doi: [10.1086/378316](https://doi.org/10.1086/378316)
- Athanassoula, E. 1992, *MNRAS*, 259, 345, doi: [10.1093/mnras/259.2.345](https://doi.org/10.1093/mnras/259.2.345)
- Athanassoula, E. 2002, *ApJL*, 569, L83, doi: [10.1086/340784](https://doi.org/10.1086/340784)
- Athanassoula, E. 2003a, in *Galaxies and Chaos*, ed. G. Contopoulos & N. Voglis, Vol. 626, 313–326, doi: [10.1007/978-3-540-45040-5_26](https://doi.org/10.1007/978-3-540-45040-5_26)
- Athanassoula, E. 2003b, *MNRAS*, 341, 1179, doi: [10.1046/j.1365-8711.2003.06473.x](https://doi.org/10.1046/j.1365-8711.2003.06473.x)
- Barazza, F. D., Jogee, S., & Marinova, I. 2008, *ApJ*, 675, 1194, doi: [10.1086/526510](https://doi.org/10.1086/526510)

- Belokurov, V., Erkal, D., Evans, N. W., Koposov, S. E., & Deason, A. J. 2018, *MNRAS*, 478, 611, doi: [10.1093/mnras/sty982](https://doi.org/10.1093/mnras/sty982)
- Belokurov, V., Sanders, J. L., Fattahi, A., et al. 2020, *MNRAS*, 494, 3880, doi: [10.1093/mnras/staa876](https://doi.org/10.1093/mnras/staa876)
- Beraldo e Silva, L., Debattista, V. P., Anderson, S. R., et al. 2023, *ApJ*, 955, 38, doi: [10.3847/1538-4357/ace976](https://doi.org/10.3847/1538-4357/ace976)
- Binney, J. 2020, *MNRAS*, 496, 767, doi: [10.1093/mnras/staa1485](https://doi.org/10.1093/mnras/staa1485)
- Binney, J., Gerhard, O. E., Stark, A. A., Bally, J., & Uchida, K. I. 1991, *MNRAS*, 252, 210, doi: [10.1093/mnras/252.2.210](https://doi.org/10.1093/mnras/252.2.210)
- Binney, J., & Tremaine, S. 2008, *Galactic Dynamics: Second Edition*
- Bland-Hawthorn, J., Tepper-Garcia, T., Agertz, O., & Freeman, K. 2023, *ApJ*, 947, 80, doi: [10.3847/1538-4357/acc469](https://doi.org/10.3847/1538-4357/acc469)
- Bonaca, A., Conroy, C., Cargile, P. A., et al. 2020, *ApJL*, 897, L18, doi: [10.3847/2041-8213/ab9caa](https://doi.org/10.3847/2041-8213/ab9caa)
- Bovy, J., Leung, H. W., Hunt, J. A. S., et al. 2019, *MNRAS*, 490, 4740, doi: [10.1093/mnras/stz2891](https://doi.org/10.1093/mnras/stz2891)
- Chen, B.-H., Kataria, S. K., Shen, J., & Guo, M. 2025, arXiv e-prints, arXiv:2510.13153, doi: [10.48550/arXiv.2510.13153](https://doi.org/10.48550/arXiv.2510.13153)
- Chen, B.-H., & Li, Z.-Y. 2022, *ApJ*, 934, 28, doi: [10.3847/1538-4357/ac795c](https://doi.org/10.3847/1538-4357/ac795c)
- Chen, B.-H., & Shen, J. 2025, *ApJ*, 990, 140, doi: [10.3847/1538-4357/adf966](https://doi.org/10.3847/1538-4357/adf966)
- Chen, B.-H., Shen, J., & Liu, Z. 2024, *ApJ*, 976, 232, doi: [10.3847/1538-4357/ad8640](https://doi.org/10.3847/1538-4357/ad8640)
- Chiba, R., Friske, J. K. S., & Schönrich, R. 2021, *MNRAS*, 500, 4710, doi: [10.1093/mnras/staa3585](https://doi.org/10.1093/mnras/staa3585)
- Conroy, C., Naidu, R. P., Zaritsky, D., et al. 2019a, *ApJ*, 887, 237, doi: [10.3847/1538-4357/ab5710](https://doi.org/10.3847/1538-4357/ab5710)
- Conroy, C., Bonaca, A., Cargile, P., et al. 2019b, *ApJ*, 883, 107, doi: [10.3847/1538-4357/ab38b8](https://doi.org/10.3847/1538-4357/ab38b8)
- Costantin, L., Pérez-González, P. G., Guo, Y., et al. 2023, *Nature*, 623, 499, doi: [10.1038/s41586-023-06636-x](https://doi.org/10.1038/s41586-023-06636-x)
- Courteau, S. 1997, *AJ*, 114, 2402, doi: [10.1086/118656](https://doi.org/10.1086/118656)
- Das, P., Hawkins, K., & Jofré, P. 2020, *MNRAS*, 493, 5195, doi: [10.1093/mnras/stz3537](https://doi.org/10.1093/mnras/stz3537)
- Debattista, V. P., Liddicott, D. J., Khachatryan, T., & Beraldo e Silva, L. 2020, *MNRAS*, 498, 3334, doi: [10.1093/mnras/staa2568](https://doi.org/10.1093/mnras/staa2568)
- Debattista, V. P., Ness, M., Gonzalez, O. A., et al. 2017, *MNRAS*, 469, 1587, doi: [10.1093/mnras/stx947](https://doi.org/10.1093/mnras/stx947)
- Debattista, V. P., & Shen, J. 2007, *ApJL*, 654, L127, doi: [10.1086/511264](https://doi.org/10.1086/511264)
- Dehnen, W. 2000, *AJ*, 119, 800, doi: [10.1086/301226](https://doi.org/10.1086/301226)
- Deng, M., Du, C., Yang, Y., Liao, J., & Ye, D. 2024, *ApJ*, 975, 28, doi: [10.3847/1538-4357/ad7799](https://doi.org/10.3847/1538-4357/ad7799)
- Di Matteo, P., Haywood, M., Lehnert, M. D., et al. 2019, *A&A*, 632, A4, doi: [10.1051/0004-6361/201834929](https://doi.org/10.1051/0004-6361/201834929)
- Du, M., Shen, J., & Debattista, V. P. 2015, *ApJ*, 804, 139, doi: [10.1088/0004-637X/804/2/139](https://doi.org/10.1088/0004-637X/804/2/139)
- Erwin, P. 2018, *MNRAS*, 474, 5372, doi: [10.1093/mnras/stx3117](https://doi.org/10.1093/mnras/stx3117)
- Eskridge, P. B., Frogel, J. A., Pogge, R. W., et al. 2000, *AJ*, 119, 536, doi: [10.1086/301203](https://doi.org/10.1086/301203)
- Farouki, R. T., & Shapiro, S. L. 1982, *ApJ*, 259, 103, doi: [10.1086/160151](https://doi.org/10.1086/160151)
- Feuillet, D. K., Feltzing, S., Sahlholdt, C. L., & Casagrande, L. 2020, *MNRAS*, 497, 109, doi: [10.1093/mnras/staa1888](https://doi.org/10.1093/mnras/staa1888)
- Fujii, M. S., Bédorf, J., Baba, J., & Portegies Zwart, S. 2018, *MNRAS*, 477, 1451, doi: [10.1093/mnras/sty711](https://doi.org/10.1093/mnras/sty711)
- Gaia Collaboration, Brown, A. G. A., Vallenari, A., et al. 2016, *A&A*, 595, A2, doi: [10.1051/0004-6361/201629512](https://doi.org/10.1051/0004-6361/201629512)
- Gaia Collaboration, Brown, A. G. A., Vallenari, A., et al. 2018, *A&A*, 616, A1, doi: [10.1051/0004-6361/201833051](https://doi.org/10.1051/0004-6361/201833051)
- Gaia Collaboration, Brown, A. G. A., Vallenari, A., et al. 2021, *A&A*, 649, A1, doi: [10.1051/0004-6361/202039657](https://doi.org/10.1051/0004-6361/202039657)
- Gaia Collaboration, Vallenari, A., Brown, A. G. A., et al. 2023, *A&A*, 674, A1, doi: [10.1051/0004-6361/202243940](https://doi.org/10.1051/0004-6361/202243940)
- Gallart, C., Bernard, E. J., Brook, C. B., et al. 2019, *Nature Astronomy*, 3, 932, doi: [10.1038/s41550-019-0829-5](https://doi.org/10.1038/s41550-019-0829-5)
- Gerhard, O. E. 1981, *MNRAS*, 197, 179, doi: [10.1093/mnras/197.1.179](https://doi.org/10.1093/mnras/197.1.179)
- Gerhard, O. E., & Vietri, M. 1986, *MNRAS*, 223, 377, doi: [10.1093/mnras/223.2.377](https://doi.org/10.1093/mnras/223.2.377)
- Gerin, M., Combes, F., & Athanassoula, E. 1990, *A&A*, 230, 37
- Ghosh, S., Saha, K., Di Matteo, P., & Combes, F. 2021, *MNRAS*, 502, 3085, doi: [10.1093/mnras/stab238](https://doi.org/10.1093/mnras/stab238)
- Grand, R. J. J., Fragkoudi, F., Gómez, F. A., et al. 2024, *MNRAS*, 532, 1814, doi: [10.1093/mnras/stae1598](https://doi.org/10.1093/mnras/stae1598)
- Grand, R. J. J., Gómez, F. A., Marinacci, F., et al. 2017, *MNRAS*, 467, 179, doi: [10.1093/mnras/stx071](https://doi.org/10.1093/mnras/stx071)
- Guo, Y., Jogee, S., Finkelstein, S. L., et al. 2023, *ApJL*, 945, L10, doi: [10.3847/2041-8213/acacfb](https://doi.org/10.3847/2041-8213/acacfb)
- Harris, C. R., Millman, K. J., van der Walt, S. é. J., et al. 2020, *Nature*, 585, 357, doi: [10.1038/s41586-020-2649-2](https://doi.org/10.1038/s41586-020-2649-2)
- Haywood, M., Di Matteo, P., Lehnert, M. D., et al. 2018, *ApJ*, 863, 113, doi: [10.3847/1538-4357/aad235](https://doi.org/10.3847/1538-4357/aad235)
- Haywood, M., Khoperskov, S., Cerqui, V., et al. 2024, *A&A*, 690, A147, doi: [10.1051/0004-6361/202348767](https://doi.org/10.1051/0004-6361/202348767)
- Helmi, A., Babusiaux, C., Koppelman, H. H., et al. 2018, *Nature*, 563, 85, doi: [10.1038/s41586-018-0625-x](https://doi.org/10.1038/s41586-018-0625-x)
- Hunter, J. D. 2007, *Computing in Science and Engineering*, 9, 90, doi: [10.1109/MCSE.2007.55](https://doi.org/10.1109/MCSE.2007.55)

- Kataria, S. K., & Vivek, M. 2024, MNRAS, 527, 3366, doi: [10.1093/mnras/stad3383](https://doi.org/10.1093/mnras/stad3383)
- Khoperskov, S., Minchev, I., Steinmetz, M., et al. 2023, arXiv e-prints, arXiv:2310.05287, doi: [10.48550/arXiv.2310.05287](https://doi.org/10.48550/arXiv.2310.05287)
- Koppelman, H. H., Helmi, A., Massari, D., Price-Whelan, A. M., & Starkenburg, T. K. 2019, A&A, 631, L9, doi: [10.1051/0004-6361/201936738](https://doi.org/10.1051/0004-6361/201936738)
- Kormendy, J., & Kennicutt, Robert C., J. 2004, ARA&A, 42, 603, doi: [10.1146/annurev.astro.42.053102.134024](https://doi.org/10.1146/annurev.astro.42.053102.134024)
- Le Conte, Z. A., Gadotti, D. A., Ferreira, L., et al. 2024, MNRAS, 530, 1984, doi: [10.1093/mnras/stae921](https://doi.org/10.1093/mnras/stae921)
- Lee, Y. H., Ann, H. B., & Park, M.-G. 2019, ApJ, 872, 97, doi: [10.3847/1538-4357/ab0024](https://doi.org/10.3847/1538-4357/ab0024)
- Li, Z., Gerhard, O., Shen, J., Portail, M., & Wegg, C. 2016, ApJ, 824, 13, doi: [10.3847/0004-637X/824/1/13](https://doi.org/10.3847/0004-637X/824/1/13)
- Li, Z., Sellwood, J. A., & Shen, J. 2017, ApJ, 850, 67, doi: [10.3847/1538-4357/aa9377](https://doi.org/10.3847/1538-4357/aa9377)
- Liu, H., Du, C., Donlon, T., & Deng, M. 2025, ApJ, 985, 4, doi: [10.3847/1538-4357/adc8a8](https://doi.org/10.3847/1538-4357/adc8a8)
- Lokas, E. L. 2018, ApJ, 857, 6, doi: [10.3847/1538-4357/aab4ff](https://doi.org/10.3847/1538-4357/aab4ff)
- Lokas, E. L., Athanassoula, E., Debattista, V. P., et al. 2014, MNRAS, 445, 1339, doi: [10.1093/mnras/stu1846](https://doi.org/10.1093/mnras/stu1846)
- Lokas, E. L., Ebrova, I., del Pino, A. s., et al. 2016, ApJ, 826, 227, doi: [10.3847/0004-637X/826/2/227](https://doi.org/10.3847/0004-637X/826/2/227)
- Long, S., Shlosman, I., & Heller, C. 2014, ApJL, 783, L18, doi: [10.1088/2041-8205/783/1/L18](https://doi.org/10.1088/2041-8205/783/1/L18)
- McGaugh, S. S., Schombert, J. M., Bothun, G. D., & de Blok, W. J. G. 2000, ApJL, 533, L99, doi: [10.1086/312628](https://doi.org/10.1086/312628)
- Menendez-Delmestre, K., Sheth, K., Schinnerer, E., Jarrett, T. H., & Scoville, N. Z. 2007, ApJ, 657, 790, doi: [10.1086/511025](https://doi.org/10.1086/511025)
- Morrow, A., Grand, R. J. J., Fragkoudi, F., & Martig, M. 2024, MNRAS, 531, 1520, doi: [10.1093/mnras/stae1250](https://doi.org/10.1093/mnras/stae1250)
- Minchev, I., & Famaey, B. 2010, ApJ, 722, 112, doi: [10.1088/0004-637X/722/1/112](https://doi.org/10.1088/0004-637X/722/1/112)
- Miwa, T., & Noguchi, M. 1998, ApJ, 499, 149, doi: [10.1086/305611](https://doi.org/10.1086/305611)
- Moetazedian, R., Polyachenko, E. V., Berczik, P., & Just, A. 2017, A&A, 604, A75, doi: [10.1051/0004-6361/201630024](https://doi.org/10.1051/0004-6361/201630024)
- Myeong, G. C., Vasiliev, E., Iorio, G., Evans, N. W., & Belokurov, V. 2019, MNRAS, 488, 1235, doi: [10.1093/mnras/stz1770](https://doi.org/10.1093/mnras/stz1770)
- Naidu, R. P., Conroy, C., Bonaca, A., et al. 2020, ApJ, 901, 48, doi: [10.3847/1538-4357/abaef4](https://doi.org/10.3847/1538-4357/abaef4)
- Naidu, R. P., Conroy, C., Bonaca, A., et al. 2021, ApJ, 923, 92, doi: [10.3847/1538-4357/ac2d2d](https://doi.org/10.3847/1538-4357/ac2d2d)
- Navarro, J. F., Frenk, C. S., & White, S. D. M. 1995, MNRAS, 275, 720, doi: [10.1093/mnras/275.3.720](https://doi.org/10.1093/mnras/275.3.720)
- Navarro, J. F., Frenk, C. S., & White, S. D. M. 1996, ApJ, 462, 563, doi: [10.1086/177173](https://doi.org/10.1086/177173)
- Negroponte, J., & White, S. D. M. 1983, MNRAS, 205, 1009, doi: [10.1093/mnras/205.4.1009](https://doi.org/10.1093/mnras/205.4.1009)
- Nepal, S., Chiappini, C., Guiglion, G., et al. 2024, A&A, 681, L8, doi: [10.1051/0004-6361/202348365](https://doi.org/10.1051/0004-6361/202348365)
- Ness, M., & Lang, D. 2016, AJ, 152, 14, doi: [10.3847/0004-6256/152/1/14](https://doi.org/10.3847/0004-6256/152/1/14)
- Nissen, P. E., & Schuster, W. J. 2010, A&A, 511, L10, doi: [10.1051/0004-6361/200913877](https://doi.org/10.1051/0004-6361/200913877)
- Noguchi, M. 1987, MNRAS, 228, 635, doi: [10.1093/mnras/228.3.635](https://doi.org/10.1093/mnras/228.3.635)
- Pettitt, A. R., & Wadsley, J. W. 2018, MNRAS, 474, 5645, doi: [10.1093/mnras/stx3129](https://doi.org/10.1093/mnras/stx3129)
- Portail, M., Gerhard, O., Wegg, C., & Ness, M. 2017, MNRAS, 465, 1621, doi: [10.1093/mnras/stw2819](https://doi.org/10.1093/mnras/stw2819)
- Quinn, P. J. 1984, ApJ, 279, 596, doi: [10.1086/161924](https://doi.org/10.1086/161924)
- Sanders, J. L., Kawata, D., Matsunaga, N., et al. 2024, MNRAS, 530, 2972, doi: [10.1093/mnras/stae711](https://doi.org/10.1093/mnras/stae711)
- Sellwood, J. A. 1981, A&A, 99, 362
- Sellwood, J. A. 2014, Reviews of Modern Physics, 86, 1, doi: [10.1103/RevModPhys.86.1](https://doi.org/10.1103/RevModPhys.86.1)
- Sellwood, J. A. 2016, ApJ, 819, 92, doi: [10.3847/0004-637X/819/2/92](https://doi.org/10.3847/0004-637X/819/2/92)
- Sellwood, J. A., & Binney, J. J. 2002, MNRAS, 336, 785, doi: [10.1046/j.1365-8711.2002.05806.x](https://doi.org/10.1046/j.1365-8711.2002.05806.x)
- Sellwood, J. A., & Gerhard, O. 2020, MNRAS, 495, 3175, doi: [10.1093/mnras/staa1336](https://doi.org/10.1093/mnras/staa1336)
- Shen, J., & Debattista, V. P. 2009, ApJ, 690, 758, doi: [10.1088/0004-637X/690/1/758](https://doi.org/10.1088/0004-637X/690/1/758)
- Shen, J., Rich, R. M., Kormendy, J., et al. 2010, ApJL, 720, L72, doi: [10.1088/2041-8205/720/1/L72](https://doi.org/10.1088/2041-8205/720/1/L72)
- Sheth, K., Melbourne, J., Elmegreen, D. M., et al. 2012, ApJ, 758, 136, doi: [10.1088/0004-637X/758/2/136](https://doi.org/10.1088/0004-637X/758/2/136)
- Simmons, B. D., Melvin, T., Lintott, C., et al. 2014, MNRAS, 445, 3466, doi: [10.1093/mnras/stu1817](https://doi.org/10.1093/mnras/stu1817)
- Springel, V. 2005, MNRAS, 364, 1105, doi: [10.1111/j.1365-2966.2005.09655.x](https://doi.org/10.1111/j.1365-2966.2005.09655.x)
- Springel, V., Pakmor, R., Zier, O., & Reinecke, M. 2021, MNRAS, 506, 2871, doi: [10.1093/mnras/stab1855](https://doi.org/10.1093/mnras/stab1855)
- Tepper-Garcia, T., Bland-Hawthorn, J., Vasiliev, E., et al. 2021, arXiv e-prints, arXiv:2111.05466, doi: [10.48550/arXiv.2111.05466](https://doi.org/10.48550/arXiv.2111.05466)
- Toomre, A. 1981, in Structure and Evolution of Normal Galaxies, ed. S. M. Fall & D. Lynden-Bell, 111–136
- Tully, R. B., & Fisher, J. R. 1977, A&A, 54, 661
- Vasiliev, E. 2019, MNRAS, 482, 1525, doi: [10.1093/mnras/sty2672](https://doi.org/10.1093/mnras/sty2672)

- Virtanen, P., Gommers, R., Oliphant, T. E., et al. 2020, Nature Methods, 17, 261, doi: [10.1038/s41592-019-0686-2](https://doi.org/10.1038/s41592-019-0686-2)
- Wylie, S. M., Clarke, J. P., & Gerhard, O. E. 2022, A&A, 659, A80, doi: [10.1051/0004-6361/202142343](https://doi.org/10.1051/0004-6361/202142343)
- Xiang, M., & Rix, H.-W. 2022, Nature, 603, 599, doi: [10.1038/s41586-022-04496-5](https://doi.org/10.1038/s41586-022-04496-5)
- Zana, T., Dotti, M., Capelo, P. R., et al. 2018, MNRAS, 473, 2608, doi: [10.1093/mnras/stx2503](https://doi.org/10.1093/mnras/stx2503)
- Zheng, Y., & Shen, J. 2025, ApJ, 979, 60, doi: [10.3847/1538-4357/ad9bae](https://doi.org/10.3847/1538-4357/ad9bae)
- Zheng, Y., Shen, J., Wu, X., & Chen, B.-H. 2025, ApJ, 986, 90, doi: [10.3847/1538-4357/adcf93](https://doi.org/10.3847/1538-4357/adcf93)
- Zhou, Y. F., Li, Z., Jiménez-Arranz, Ó., Roca-Fàbrega, S., & et al. 2025, in preparation